Japanese Journal of Applied Physics **62**, SD1013 (2023) **REGULAR PAPER**
https://doi.org/**10.35848/1347-4065/aca912**

Effect of morphology on the phonon thermal conductivity in Si/Ge superlattice nanowires

Ivan I. Khaliava[1], Alexander L. Khamets[1], Igor V. Safronov[2], Andrew B. Filonov[1], Takashi Suemasu[3], and Dmitri B. Migas[1,4*]

[1]*Belarusian State University of Informatics and Radioelectronics, 220089 Minsk, Belarus*
[2]*Belarusian State University, 220030 Minsk, Belarus*
[3]*Department of Applied Physics, Faculty of Pure and Applied Sciences University of Tsukuba, Tsukuba 305-8573, Japan*
[4]*National Research Nuclear University MEPhI (Moscow Engineering Physics Institute), Kashirskoe shosse 31, 115409 Moscow, Russia*

*E-mail: migas@bsuir.by

Received October 11, 2022; revised November 28, 2022; accepted December 5, 2022; published online December 30, 2022

We used nonequilibrium molecular dynamics to investigate the role of morphology in the phonon thermal conductivity of ⟨100⟩, ⟨110⟩, ⟨111⟩ and ⟨112⟩-oriented Si/Ge superlattice nanowires at 300 K. Such nanowires with ⟨112⟩ growth direction were found to possess the lowest values of the thermal conductivity [1.6 W/(m·K) for a Si and Ge segment thickness of ∼3 nm] due to the lowest average group velocity and highly effective {113} facets and Si/Ge(112) interface for phonon-surface and phonon-interface scattering, respectively. Comparison with homogeneous and core/shell Si and Ge nanowires showed that the superlattice morphology is the most efficient to suppress the thermal conductivity.

1. Introduction

Efficient direct conversion of heat into electricity is the key issue to promoting thermoelectric devices.[1)] The efficiency of thermoelectric energy conversion is determined by the dimensionless value ZT or thermoelectric figure of merit, defined as $S^2\sigma T/(\kappa_L + \kappa_e)$, where S, σ, T and κ_L, κ_e are the Seebeck coefficient, electrical conductivity, operating temperature and thermal conductivity (phonon/lattice and electronic components), respectively.[2)] Nowadays, much effort has been focused on thermal transport in low-dimensional semiconductor materials due to the possibility to reduce κ_L compared to their bulk counterparts by introducing additional scattering of phonons on surfaces and interfaces.[3–9)] For example, in Ref. 7 the decrease in κ_L to several tenths of W/(m·K) for the natural superlattice $(Bi_2)_m(Bi_2Te_3)_n$ is due to strong phonon resonance scattering caused by low-frequency optical and heat-carrying acoustic phonon coupling, as well as lattice anharmonicity. An anomalous κ_L reduction below the amorphous limit was also investigated for connected Si nanodots[8)] in the form of oriented nanocrystals separated by an ultrathin amorphous layer, where significant phonon scattering occurs. The phononic patterning design of a poly-Si membrane showed a 60% decrease in κ_L because of an increase in incoherent phonon boundary scattering and, as a consequence, a twofold increase in the ZT value.[9)] Among such low-dimensional materials, nanowires (NWs) also attract attention, and in particular, Si and Ge NWs, which are characterized by sufficiently high mobility of charge carriers.[10,11)] Si and Ge NWs have been studied extensively,[10–21)] since Si and Ge are common materials in microelectronics. Numerical estimates of κ_L of homogeneous Si and Ge nanowires are in the range of ∼10−25 W/(m·K) and ∼6−14 W/(m·K), respectively,[15,16,19)] and these values are an order of magnitude less than the one for Si and Ge bulks (∼140 W/(m·K)[22)] and ∼55 W/(m·K),[23)] respectively). Experimental measurements demonstrate even lower values of κ_L for Si NWs (∼1–10 W/(m·K)[24,25)]) and Ge NWs (∼1.5−2.2 W/(m·K)[26)]) caused by a rather high surface roughness and the appearance of amorphous oxide layers on the surface.[25,26)] However, these defects led not only to a decrease in the total thermal conductivity but also to a decrease in the power factor ($S^2\sigma$) and ZT values. In addition, results of theoretical[13,19,20)] and experimental[24–26)] studies show that κ_L of NWs increases with diameter pointing out variation in the diameter of a NW to be a feasible way to change κ_L. It is also theoretically demonstrated that the interface can provide an additional reduction in κ_L for Si/Ge superlattice NWs (with alternating Si and Ge segments along the NW axis) compared with homogeneous NWs[13,15,16,19,21)] mainly considering ⟨100⟩-oriented NWs with square or round cross-sections. Moreover, the appearance of {110} facets provided larger κ_L.[18)] As we have already demonstrated in our previous work[27)] for Si, Ge, and Si/Ge core/shell NWs, morphology can sizably affect κ_L values in these NWs by varying facets and orientations (⟨100⟩, ⟨110⟩, ⟨111⟩, ⟨112⟩). In particular, for Si/Ge core/shell NWs with diameters of ∼5.5 nm the changes in κ_L can reach ∼34%–45% [or 2.5 −3.9 W/(m·K)]. At the same time, it is found that the appearance of {100}, {112}, and {113} facets led to a decrease in κ_L, while the opposite effect is observed by introducing {110} and {111} facets. The lowest values of κ_L for Si/Ge core/shell NWs were estimated to be 7.62, 9.22, 7.18, and 5.76 W/(m·K) for ⟨100⟩, ⟨110⟩, ⟨111⟩and ⟨112⟩ orientations, respectively, also indicating anisotropy with respect to the crystallographic directions.[27)]

The aim of this work is to extend our previous study by introducing a Si/Ge interface perpendicular to a NW axis (instead of a Si/Ge interface parallel to a NW axis for the core/shell morphology[27)]) in Si/Ge superlattice NWs and monitor changes in κ_L, since Si/Ge superlattice NWs can be easily fabricated.[28)]

2. Simulation techniques

We considered ⟨100⟩-, ⟨110⟩-, ⟨111⟩- and ⟨112⟩-oriented Si/Ge superlattice NWs in the form of periodic and symmetric arrangement of segments with sharp interfaces (excluding interdiffusion) and diameters of about 5.5 nm. Two segments in length (adjacent Si and Ge ones) served as a period and the minimum period corresponded to 8 and 12 monolayers for

NWs with ⟨100⟩, ⟨110⟩ and ⟨111⟩, ⟨112⟩ orientations, respectively. The period was a variable parameter. Since the detailed ab initio study on the role of morphology on the stability of Si NWs has been already performed,[29,30] we introduce {100} and {110} facets for ⟨100⟩ orientations, {100}, {110} and {111} facets for ⟨110⟩ orientations, {110} and {112} facets for ⟨111⟩ orientations, and, eventually, {110}, {111} and {113} facets for ⟨112⟩ orientations. Surface reconstruction of the facets has been done by forming dimers on {100}, {112}, and {113} facets like in ab initio study[29,30] to assure that there is no surface atom with two dangling bonds. No H atoms were used to saturate dangling bonds.

The total energy of the investigated NWs was initially minimized by molecular statics implemented in the LAMMPS software package,[31] by relaxing and optimizing the atomic structure with a variable supercell. Three-dimensional periodic boundary conditions with a vacuum gap of ~20 nm in the NW cross-sectional plane were used. The interatomic interaction for the Si-Ge system was described by using the Tersoff potential.[32] This potential is common in thermal conductivity simulations of Si/Ge NWs.[13,15,16,19–21]

The method of nonequilibrium molecular dynamics, also implemented in LAMMPS, was used to simulate phonon thermal conductivity at 300 K. The time step was set to 1 fs. Initially, the structures were brought into thermodynamic equilibrium using isobaric-isothermal and canonical ensembles for 0.1 ns each at 300 K. Then, a microcanonical ensemble was used for 2 ns to establish thermodynamic equilibrium. To control and maintain the temperature in the structures, the Langevin thermostats were used, and the corresponding damping coefficients were introduced (for Ge atoms it is equal to 1, for Si atoms it is equal to 2.586), which affected the relaxation time during vibrations due to the difference in the atomic masses. To introduce a temperature gradient, two thermostats were used: cold (290 K) and hot (310 K) ones placed at a distance of half the supercell size in the direction of heat flow propagation (along the NW axis). The size of the supercell (which is equivalent to the NW length) was set to ~100 nm (see for details[27]). To reduce temperature fluctuations in the thermostat regions, the number of atoms was kept equal to about 4464, which is sufficient to stabilize the temperature. The phonon thermal conductivity (κ_L) along the NW axis was determined from Fourier's law:

$$\kappa_L = -\frac{E}{2S_{sec} \cdot t \cdot (dT/dz)},$$

where E is the transferred thermal energy; 2 is the coefficient associated with the heat flow propagation in two directions due to periodic boundary conditions; t is the simulation time; S_{sec} is the cross–sectional area; dT/dz is the temperature gradient in the longitudinal direction. We also checked that 2 ns of simulation are enough to reach the steady state. The cross-sectional area was estimated using the ratio of the NW volume to its height. The volume of NWs was estimated as the sum of atomic volumes.

The vibrational density of states (VDOS) was calculated using the auxiliary postprocessing code PHANA[33] (PHonon ANAlyzer for Fix-Phonon) from LAMMPS molecular dynamic data after 20 ns of equibrilization with the isobaric-isothermal ensemble.

3. Results and discussion

In nanostructures phonons can be effectively scattered on different facets[12,18] and interfaces,[13,15,16,19–21] where each facet or interface provides its own contribution, in addition to possible anisotropy in heat propagation along different orientations.[14] Thus, it is not so straightforward to analyze (especially quantitatively) a dependence of κ_L with respect to the morphology of a nanostructure because calculations of the effective phonon transmission coefficients and thermal boundary resistances are necessary,[34] which is beyond the scope of this work. Nevertheless, we'd like to discuss, at least qualitatively, some interesting features of heat propagation in Si/Ge superlattice NWs in comparison with Si, Ge, and Si/Ge core/shell NWs. Figure 1 presents the results of κ_L simulation for ⟨100⟩-, ⟨110⟩-, ⟨111⟩-, ⟨112⟩-oriented Si/Ge superlattice NWs with respect to the period. It was found that NWs with the ⟨111⟩ and ⟨110⟩ axes displayed the highest values of κ_L, whereas the lowest values were typical of NWs with ⟨112⟩ axes. As a general trend, κ_L increases with period indicating that the less dense sequence of the Si/Ge interfaces provides the less intensive phonon scattering. The presence of the Si/Ge interfaces indeed led to κ_L suppression since for homogeneous Ge and Si NWs with comparable morphology and diameters κ_L values at 300 K were estimated to be about 8–11 and ~14–19 W/(m·K) depending on the orientation, respectively,[27] pointing out effective phonon scattering at the interfaces if the period was smaller than 40 nm (Fig. 1). For the cases with the period of more than 40 nm, Si segments, which possess larger values of κ_L than Ge ones, start defining κ_L in Si/Ge superlattice NWs. Thus, there is a delicate balance between the contributions of more heat-conducting Si segments and phonon-interface scattering to define κ_L in such nanostructures. Anisotropy in κ_L for Si/Ge superlattice NWs has been also predicted where ⟨110⟩- and ⟨111⟩-oriented NWs were found to have the highest and lowest values of κ_L.[11] Such a difference with respect to our results can stem from the fact that in Ref. 11, the asymmetric arrangement of Si/Ge segments along the NW axis was considered in addition to the sizably smaller diameters (less than 2 nm) and passivation by hydrogen.

The dependences in Fig. 1 also demonstrate the presence of minima in the κ_L values at periods in the range of ~3–4 nm which are 2.00, 2.21, 3.23 and 1.57 W/(m·K) for ⟨100⟩, ⟨110⟩, ⟨111⟩ and ⟨112⟩ orientations, respectively. Similar trends in κ_L for Si/Ge superlattice NWs with sharp interfaces have been found earlier only for ⟨100⟩- and ⟨111⟩-oriented NWs.[13,15,19–21] The appearance of such minima is associated with a change in the heat transfer mechanism from incoherent to coherent, which is discussed in detail elsewhere.[13,15,20,21,35] Note that the minimum values of thermal conductivity for each orientation are achieved at different periods—when they are equal to the phonon coherence length.[36] The results obtained can be explained qualitatively based on the vibrational density of states (VDOS) of atoms that belong to the surface, interface, and volume (inside the Si or Ge segment) regions (Fig. 2). The most significant difference in VDOS for Si/Ge superlattice NWs with different orientations is observed for interface

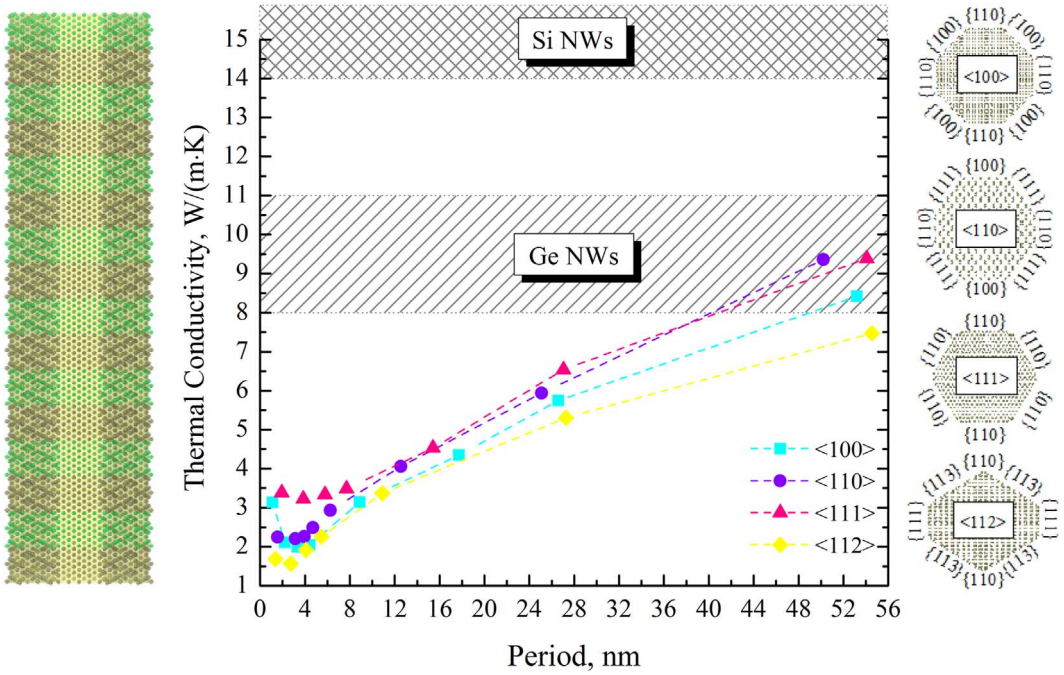

Fig. 1. (Color online) Phonon thermal conductivity at 300 K versus period for Si/Ge superlattice NWs with different morphologies. Lines connecting points are the guide to the eye. The shaded areas show a range of thermal conductivity values for homogeneous NWs with different orientations. The cross-sections of NWs with different morphologies and a NW lateral view to trace a period are also shown.

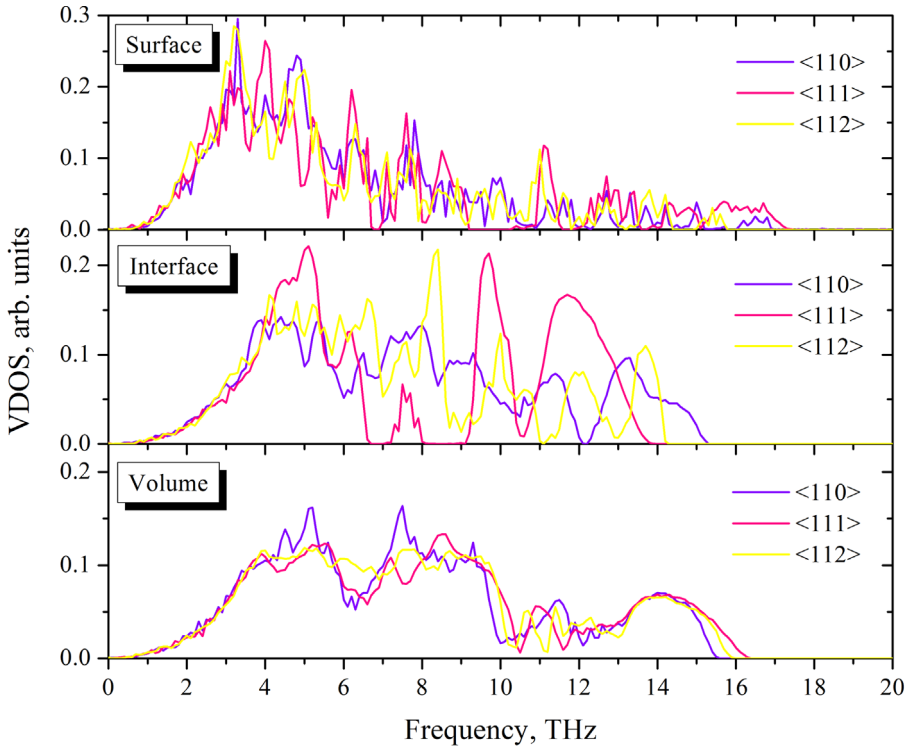

Fig. 2. (Color online) VDOS of surface, interface and volume atoms at 300 K for Si/Ge superlattice NWs with different orientations.

atoms, while for surface atoms the difference in VDOS is marginal, indicating interfaces to play a major role in anisotropy of heat transfer in such nanostructures. ⟨111⟩-oriented Si/Ge superlattice NWs are characterized by the presence of several well-resolved (and sometimes separated) peaks with the largest values of interface VDOS compared to other orientations (Fig. 2), which can be associated with the lowest phonon-interface scattering and, as a result, the largest κ_L (Fig. 1). A similar analysis was carried out in Ref. 37 when comparing the VDOS for pure Si and Si-core/Ge-shell NWs. Contrary, ⟨112⟩-oriented superlattice NWs, which have the lowest κ_L, are characterized by the presence of multiple peaks. As it is shown in Ref. 38, such frequency dispersion indicates more flattened dispersion curves and, as a consequence, a lower phonon group velocity[14)] leading to the lowest κ_L.

We have also checked how some specific facets can affect phonon scattering and, as a consequence, κ_L values. Possible morphologies of Si/Ge superlattice NWs along with changes

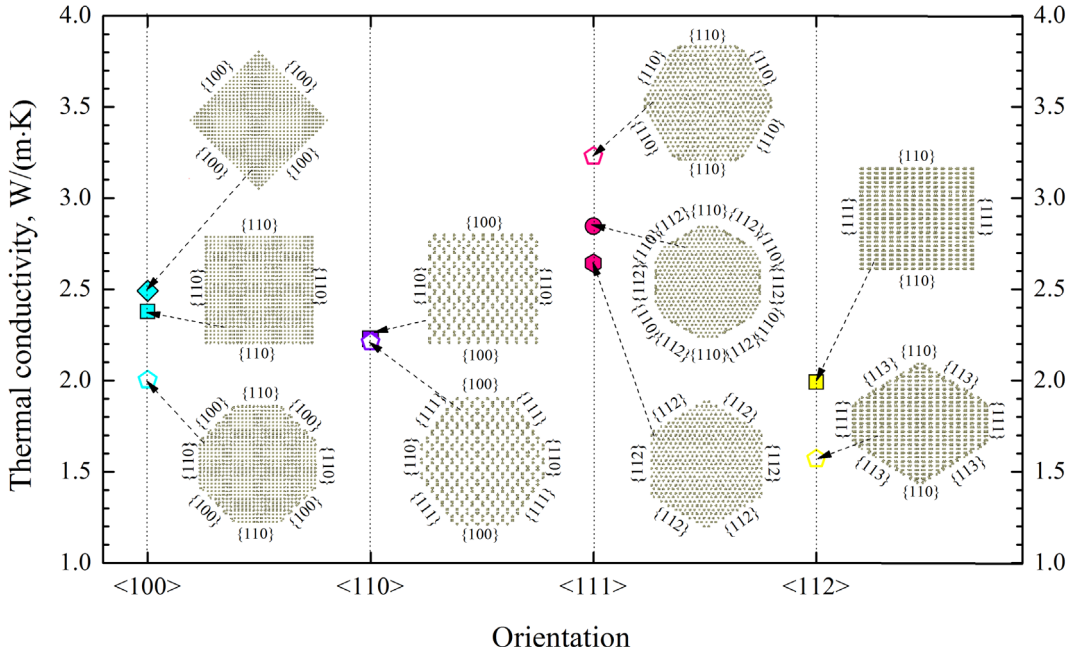

Fig. 3. (Color online) Effect of different facets on phonon thermal conductivity at 300 K for Si/Ge superlattice NWs with different orientations.

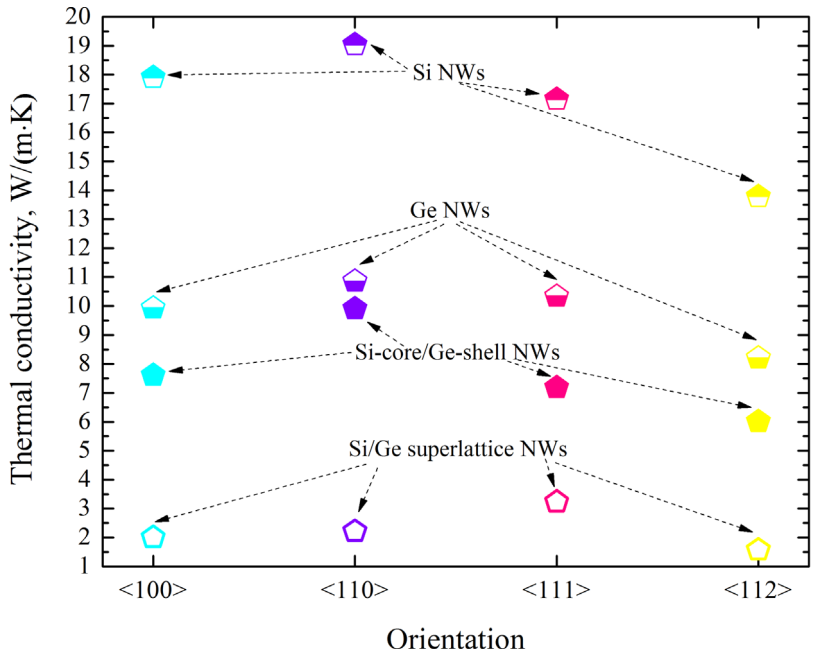

Fig. 4. (Color online) Effect of orientation on thermal conductivity for different NWs. Data for homogeneous Si, Ge and Si-core/Ge-shell NWs are from.[27)]

in κ_L are presented in Fig. 3. For this analysis we have selected NWs with the lowest κ_L values according to Fig. 1. It is evident that the appearance of {113} facets for ⟨112⟩ oriented NWs and {112} facets for ⟨111⟩ oriented NWs intensifies phonon scattering and provides lowering in κ_L. Contrarily, {111} and {110} facets are inefficient in phonon scattering in perfect agreement with our previous results for homogenous Si and Ge NWs as well as for Si/Ge core/shell NWs.[27)] The origin of this effect can be associated with the interplay between the diffuse and specular scattering of phonons from the {113} and {112} facets due to their surface reconstruction.[12)] For Si/Ge superlattice NWs the change in κ_L with morphology can reach only ∼20% (or 0.5 W/(m·K)), which is about 2 times lower compared to the Si-core/Ge-shell NWs, which emphasizes the significant influence of interfaces.

Eventually, it is very interesting to compare changes in κ_L for homogenous Si and Ge NWs and Si/Ge superlattice and core/shell NWs with different orientations (see Fig. 4). For this analysis we used Si/Ge superlattice NWs with the periods in the range of ∼3–4 nm and Si-core/Ge-shell NWs with a core volume fraction of ∼10%–30%[27)] which displayed the lowest κ_L values. It is clear that ⟨112⟩-oriented NWs, independently of homogenous or heterogeneous morphology, are characterized by the lowest κ_L values. In addition, we found that κ_L values change with respect to orientation by 1.7, 3.5, 5.0, and 3.0 W/(m·K) for Si/Ge superlattice, Si-core/Ge-shell, Si, and Ge NWs, respectively. It is also evident that

the more efficient phonon-interface scattering is typical of Si/Ge superlattice NWs rather than for Si/Ge core/shell NWs.

4. Conclusions

By means of nonequilibrium molecular dynamics, we have investigated how morphology affected the phonon thermal conductivity in Si/Ge superlattice NWs with ⟨100⟩, ⟨110⟩, ⟨111⟩, and ⟨112⟩ growth directions at 300 K indicating ⟨112⟩-oriented NWs to possess the lowest values of κ_L ∼1.6 W/(m·K) for a period of ∼3 nm. Comparison with homogeneous and core/shell Si and Ge NWs showed that the influence of morphology on the thermal conductivity is less significant for Si/Ge superlattice NWs. The latter may be due to the prevailing of the efficient phonon-interface mechanism in phonon scattering. The results of the study point out perspectives of Si/Ge superlattice NWs for thermoelectric device fabrication.

Acknowledgments

This work has been supported by the Belarusian National Research Program "Materials science, new materials and technology." D.B. Migas acknowledges the support of the MEPhI Program Priority 2030. The resources of NRNU MEPhI high-performance computing center were used for this study.

1) Y. Li, G. Wang, M. Akbari-Saatlu, M. Procek, and H. H. Radamson, Front. Mater. **8**, 611078 (2021).
2) A. F. Ioffe, *Physics of Semiconductors* (Academic Press Inc, New York, 1960) 1st ed., p. 436.
3) S.-M. Lee, D. G. Cahill, and R. Venkatasubramanian, Appl. Phys. Lett. **70**, 2957 (1997).
4) T. Borca-Tasciuc et al., Superlat. Microstruct. **28**, 199 (2000).
5) W. L. Liu, T. Borca-Tasciuc, G. Chen, J. L. Liu, and K. L. Wang, J. Nanosci. Nanotech. **1**, 39 (2001).
6) S. Chakraborty, C. A. Kleint, A. Heinrich, C. M. Schneider, J. Schumann, M. Falke, and S. Teichert, Appl. Phys. Lett. **83**, 4184 (2003).
7) H. Zhu, C. Zhao, P. Nan, X.-M. Jiang, J. Zhao, B. Ge, C. Hiao, and Y. Xie, Chem. Mater. **33**, 1140 (2021).
8) Y. Nakamura et al., Nano Energy **12**, 845 (2015).
9) R. Yanagisawa, N. Tsujii, T. Mori, P. Ruther, O. Paul, and M. Nomura, Appl. Phys. Express **13**, 095001 (2020).
10) X. Chen, Z. Wang, and Y. Ma, J. Phys. Chem. C **115**, 20696 (2011).
11) M. Shelley and A. A. Mostofi, EPL **94**, 67001 (2011).
12) F. Sansoz, Nano Lett. **11**, 5378 (2011).
13) M. Hu and D. Poulikakos, Nano Lett. **12**, 5487 (2012).
14) H. Karamitaheri, N. Neophytou, M. K. Taher, R. Faez, and H. Kosina, J. Electron. Mater. **42**, 2091 (2013).
15) X. Mu, L. Wang, X. Yang, P. Zhang, A. C. To, and T. Luo, Sci. Rep. **5**, 16697 (2015).
16) A. Ozden, A. Kandemir, F. Ay, N. K. Perkgoz, and C. Sevik, J. Electron. Mater. **45**, 1594 (2016).
17) A. Porter, C. Tran, and F. Sansoz, Phys. Rev. B **93**, 195431 (2016).
18) Y. Zhou, Y. Chen, and M. Hu, Sci. Rep. **6**, 24903 (2016).
19) A. Kandemir, A. Ozden, T. Cagin, and C. Sevik, Sci. Technol. Adv. Mater. **18**, 187 (2017).
20) N. Samaraweera, J. M. Larkin, K. L. Chan, and K. Mithraratne, J. Appl. Phys. **123**, 244303 (2018).
21) C. W. Zhang, H. Zhou, Y. Zeng, L. Zheng, Y. L. Zhan, and K. D. Bi, Int. J. Heat Mass Transf. **132**, 681 (2019).
22) H. R. Shanks, P. D. Maycock, P. H. Sidles, and G. C. Danielson, Phys. Rev. **130**, 1743 (1963).
23) A. F. Ioffe, Can. J. Phys **34**, 1342 (1956).
24) D. Li, Y. Wu, R. Fan, P. Yang, and A. Majumdar, Appl. Phys. Lett. **83**, 3186 (2003).
25) A. I. Hochbaum, R. Chen, R. D. Delgado, W. Liang, E. C. Garnett, M. Najarian, A. Majumdar, and P. Yang, Nature **451**, 163 (2008).
26) M. C. Wingert, Z. C. Chen, E. Dechaumphai, J. Moon, J. H. Kim, J. Xiang, and R. Chen, Nano Lett. **11**, 5507 (2011).
27) I. I. Khaliava, A. L. Khamets, I. V. Safronov, A. B. Filonov, and D. B. Migas, Semiconductors **6**, 428 (2022).
28) C. Jia, Z. Lin, Y. Huang, and X. Duan, Chem. Rev. **119**, 9074 (2019).
29) D. B. Migas and V. E. Borisenko, J. Appl. Phys. **105**, 104316 (2009).
30) D. B. Migas, V. E. Borisenko, Rusli, and C. Soci, Nano Converg. **2**, 16 (2015).
31) S. Plimpton, J. Comp. Phys. **117**, 1 (1995).
32) J. Tersoff, Phys. Rev. B **39**, 5566 (1989).
33) L. T. Kong, Comput. Phys. Commun. **182**, 2201 (2011).
34) E. T. Swartz and R. O. Pohl, Rev. Mod. Phys. **61**, 605 (1989).
35) M. V. Simkin and G. D. Mahan, Phys. Rev. Lett. **84**, 927 (2000).
36) B. Latour, S. Volz, and Y. Chalopin, Phys. Rev. B **90**, 014307 (2014).
37) M. Hu, K. P. Giapis, J. V. Goicochea, X. Zhang, and D. Poulikakos., Nano Lett. **11**, 618 (2011).
38) J. M. Skelton, L. A. Burton, A. J. Jackson, F. Oba, S. C. Parker, and A. Walsh, Phys. Chem. Chem. Phys. **19**, 12452 (2017).